Eur. J. Mineral., 36, 749–765, 2024
https://doi.org/10.5194/ejm-36-749-2024

European Journal of Mineralogy
Open Access

When detection and quantification of mineral fibres in natural raw materials are at their limit – the case of a clay from the Gomsiqe–Puka mining area (Albania)

Alessandro F. Gualtieri[1], Simona Marchetti Dori[1], Daniele Malferrari[1], Tommaso Giovanardi[1], Riccardo Fantini[1], Francesco Colombo[1], Mattia Sisti[1], Rossella Arletti[1], Maria Cristina Gamberini[2], Eleonora Braschi[3], Andrea Orlando[3], and Enrico Mugnaioli[4,5]

[1]Department of Chemical and Geological Sciences, University of Modena and Reggio Emilia, Modena, 41125, Italy
[2]Department of Life Sciences, University of Modena and Reggio Emilia, Modena, 41125, Italy
[3]C.N.R. – I.G.G. – U.O.S., Florence, 50121, Italy
[4]Earth Sciences Department, University of Pisa, Pisa, 56126, Italy
[5]CISUP, University of Pisa, Pisa, 56126, Italy

Correspondence: Alessandro F. Gualtieri (alessandro.gualtieri@unimore.it)

Received: 3 June 2024 – Revised: 16 July 2024 – Accepted: 23 July 2024 – Published: 10 September 2024

Abstract. In today's global market, the movement of raw materials and goods in the free global market can lead to unintended consequences. One significant concern is the potential presence of contaminants and carcinogens, particularly when products originate from regions with less strict regulations and enforcement. This issue is particularly pertinent in the natural raw materials utilized in the global building materials market, where contamination by asbestos minerals can occur. Therefore, the screening of natural raw materials for asbestos content is crucial to mitigate the risk of exposure to carcinogens for both workers and the general public. In this study, we examine a challenging case involving a smectite–kaolinite clay from Gomsiqe–Puka, Albania, possibly containing mineral fibres. Detection and quantification of asbestos in this material push the boundaries of current experimental methods. Using transmission electron microscopy (TEM), micro-Raman spectroscopy, and electron probe microanalysis (EPMA), we identified the presence of asbestos tremolite, along with a rare fibrous variety of diopside. EPMA data allowed the advancement of some speculations on the origin of the observed tremolites, showing that Al-rich tremolites are typical of oceanic settings and Al-poor tremolites are more similar to continental tremolites.

We also investigated the impact of milling on the detection and quantification of mineral fibres, testing different milling times. This investigation is crucial as it can influence the classification of the raw material as asbestos-containing material or not. Our findings indicate that tremolite, cleavage fragments, and elongated particles break down into smaller World Health Organization (WHO) fibres with increasing milling times (1–5 min). However, prolonged milling (10 min) leads to overgrinding, resulting in a decrease in the number of counted WHO fibres with a length exceeding 5 µm.

1 Introduction

The family of recognized asbestos minerals includes chrysotile (serpentine asbestos) and five amphibole species (asbestos actinolite, "amosite", asbestos anthophyllite, "crocidolite", and asbestos tremolite) (Gualtieri et al., 2022). These six minerals are classified by the International Agency for Research on Cancer (IARC) as Group 1 carcinogens. Asbestos minerals can occasionally contaminate natural raw materials exploited, marketed, and used in the global market of building materials. In most of the European countries, if asbestos is detected in a raw material or in any other commercial product, regardless of the concentration, that material is considered illegal (Italian Law No. 257/1992). In the past, we reported the contamination of asbestos tremolite in a sodium feldspar exploited from the Orani mine in Sardinia (Italy) (Gualtieri et al., 2018a) and used for about 40 years for the production of stoneware tiles, the contamination of commercial brucite with chrysotile (Malferrari et al., 2021), and the contamination of chrysotile in commercial magnesite (Gualtieri et al., 2023b).

Since the presence of asbestos can classify a raw material as illegal, it is critical to define what we mean by the term "asbestos". Unfortunately, to date the issue of a globally shared definition of "asbestos" is still open. Recently, the International Mineralogical Association (IMA) Working Group on "Asbestos, asbestiform minerals, and other respirable minerals that pose potential negative health risks" was unable to come to an agreement given the polarization of views on several key definitions, including "asbestos". The unshared definition of "asbestos" that the working group came out with has been the following:

> A generic term applied to the asbestiform variety of serpentine (chrysotile) and the asbestiform variety of amphibole group minerals (anthophyllite, cummingtonite–grunerite, tremolite–actinolite and riebeckite), which have been exploited, prospected, described in the literature, traded and sold commercially for their unique physical properties resulting from fibril dimension 0.5 μm or smaller in width (Gualtieri et al., 2023a).

The challenge escalates in scenarios where the presence of asbestos nears the detection limits of experimental techniques. In such instances, sample preparation can significantly influence detection analysis outcomes. Although extensively discussed in the literature, the issue of sample preparation, especially the grinding and milling steps impacting the number and morphometry of detected mineral fibres, remains contentious. Indeed, sample preparation alters particle morphology crucial for characterizing, defining, and distinguishing asbestos minerals (Siegrist and Wylie, 1980; Schneider et al., 1998). For instance, the Occupational Safety and Health Administration (OSHA) earlier defined an asbestos fibre as any particle of anthophyllite, tremolite, actinolite chrysotile, "amosite", or "crocidolite" > 5 µm with an aspect ratio (length / width) ≥ 3 (NIOSH, 1972). Among the various sample preparation methods, elutriation can be used to separate the fine fraction from a heterogeneous sample avoiding the grinding of the raw sample. It is obtained by injecting a stream of gas or liquid through the soil sample, which can extract mineral fibres among other particulate materials (Malinconico et al., 2022). An asbestos elutriator was designed by Berman and Kolk (1997) for USEPA, but other methods are available such as the ISO 22262-2 (2014) guideline.

Spurny et al. (1980) reported that mechanical and ultrasound treatments of asbestos and glass fibres may induce changes in their physical and chemical properties. Milling alters not only size distribution but also particle shape and crystal structure of asbestos fibres. Early studies by Wylie and Schweitzer (1982) on wollastonite fibres demonstrated that the accuracy of shape characterization can be influenced by various factors, including sieving and instrumentation, while different grinding methods have minimal effects on fibrosity. These authors found that prolonged grinding times tend to produce slightly wider, less elongated wollastonite particles.

In their recent comprehensive review, Malinconico et al. (2022) noted that the outcome of comminution of a natural sample depends on the species (e.g. serpentines vs. amphiboles) and their variety. For presumably non-fibrous amphiboles, extended milling times induce the formation of cleavage fragments, from fracturing massive prismatic amphiboles that can produce non-parallel side elongated particles with steps, and alter both morphology and fibre concentration (Bloise et al., 2018a; Baietto et al., 2019). For tremolite and anthophyllite asbestos, an increase in lattice strain and a decrease in crystallinity were reported after just 30 s of grinding (Bloise et al., 2018b). With longer milling times (> 10 min), the lengths of asbestos amphiboles are likely to fall below the World Health Organization (WHO) length limit of 5 µm (WHO, 1986; Bloise et al., 2018b). Consequently, grinding time can significantly influence analytical results (leading to over- or underestimation) when quantifying only respirable fibres in a sample.

Baietto (2019) also investigated the behaviour of asbestiform and non-asbestiform (prismatic) tremolite subjected to mechanical actions, focusing on morphology changes post-grinding. Initially fibrous tremolite particles exhibited reduced fibrosity after grinding, as the production of prismatic elements became predominant. In turn, samples initially rich in prismatic particles further increased in prismaticity.

Regarding chrysotile, variations were observed between wet and dry grinding, with wet grinding promoting the separation of chrysotile fibres into thin fibrils, while dry grinding tended to break fibres, reducing aspect ratios (Salamatipour et al., 2016).

Belardi et al. (2018) argued that commonly used counting criteria for asbestos identification should not solely rely on particle morphometric characteristics (length, width, etc.),

as identifying asbestos fibres in dust generated after mechanical stresses requires a multidisciplinary/multiscale approach. These authors also found that using dimensional criteria based only on particle width and aspect ratio may lead to misidentification among different fibrous and non-fibrous particles (Belardi et al., 2018).

In this study, we present a complex case study of a plastic clay raw material extracted from the Gomsiqe–Puka mine (Albania), unexpectedly containing mineral fibres, with controversial detection and quantification of asbestos. X-ray powder diffraction analyses (with an estimated lower detection limit of ca. 0.5 wt %) on the raw sample revealed the presence of smectite and illite as major phases. Minor mineral fibres were discovered through transmission electron microscopy, micro-Raman, and electron probe microanalysis. Various fibre species, including "asbestos" regulated ones, were observed and classified based on their crystal chemical and morphological characteristics. We systematically investigated the effect of milling on fibre liberation, detection, and counting at different milling times, aiming to shed light on the influence of sample grinding on asbestos fibre identification and quantification.

2 Experimental part

2.1 Description of the natural material

The sample used in this study is a clay from the mining area of Gomsiqe–Puka (Albania). This clay is mined as kaolin and can be used as a component for the manufacture of traditional ceramic tiles (Dondi et al., 2014). This kaolinite-rich clay is an alteration product affecting gabbros and basalts of the ophiolitic Mirdita unit and has been ascribed to a Pliocene–Quaternary episode, although weathering of their paleosoils could be older (Saccani and Tassinari, 2015; Nicolas et al., 2017).

The Mirdita unit (Saccani and Tassinari, 2015) is connected to the Dinaric ophiolites to the north and to the Pindos ophiolites in Greece to the south (Hoeck et al., 2002). The ophiolites of the Mirdita unit represent remnants of the Mesozoic oceanic lithosphere within the Dinaride–Ellenide segment of the Alpine orogenic system and can be divided into a western (WMO) and an eastern (EMO) domains, differentiated by stratigraphy, petrography, and geochemistry (Saccani and Tassinari, 2015). Both ophiolitic domains originated during the Middle–Upper Jurassic (161.2 ± 4.0 to 145.5 ± 4.0 Ma). The western massifs in the northern Mirdita area (including Gomsiqe and Puka) are mantle domes, variously covered by a horizon of milonitic plagioclase–amphibole peridotites. The western slopes of the Puka massif are occupied by highly altered gabbros, locally covered by unformed pillow basalts (Nicolas et al., 2017). Serpentinization phenomena in these rocks can lead to the formation of fibrous minerals such as chrysotile and amphiboles of the actinolite–tremolite series. Because clay-rich deposits affecting gabbros and basalts of the ophiolitic Mirdita unit are in tectonic contact with the serpentinized peridotite formations (Nicolas et al., 2017), contamination of the clays by fibrous minerals is possible.

A representative batch of 5 kg of this raw material has been provided for the study.

2.2 Experimental methods for the characterization of the material

The mineralogical characterization of the sample was performed by X-ray powder diffraction (XRPD) using an X'Pert PRO PANanalytical θ/θ diffractometer (CuKα radiation, 40 kV and 40 mA), equipped with a real-time multiple-strip detector and Ni filter on the secondary beam path. A 1/4° divergence slit and a 1/4° antiscatter slit were used. Data were collected from 3 to 80° 2θ, with a virtual scan time of 50 s per step and step scan of 0.0167° 2θ. Qualitative phase analysis was possible using the X-Pert High Score Plus software.

Thermogravimetric (TG) experiments were conducted using a Seiko SSC/5200 thermal analyser coupled with a quadrupole mass spectrometer (ESS, GeneSys Quadstar 422) to analyse gases released during thermal reactions (MSEGA). Gas sampling was carried out through an inert fused silicon capillary system, which was maintained at elevated temperature to prevent gas condensation. Analysis of chemical species evolved with temperature was performed with background subtraction to establish baseline conditions before gas analysis.

The experimental parameters included a heating rate of 10 °C min^{-1}, a heating range from 25 to 1050 °C, and data acquisition every 0.5 s. To also obtain mass analyses of the evolved gases, a second measurement was taken in the same thermal range at a heating rate of 20 °C min^{-1} purging with helium gas at a flow rate of 100 µL min^{-1}. The mass analysis used the multiple ion detection mode, focusing on m/z ratios 17 and 18 for H_2O, 30 for NO, 44 for CO_2, and 64 for SO_2. Mass measurements were carried out using a secondary electron multiplier detector at 900 V with an integration time of 1 s for each mass measured.

Preliminary observation of the elongated particles in the sample was done with a Meiji Techno stereomicroscope (50×). Elongated particles and fibrous-like aggregates that were identified were gently picked up to preserve their morphology using tweezers and subsequently characterized with electron microscopy and micro-Raman (see below).

Micro-Raman analyses were conducted on the aggregates separated using the optical microscope with the confocal micro-Raman LabRAM HR Evolution (Horiba Jobin Yvon, Edison, NJ, USA). It was equipped with a red He–Ne laser at 532 nm (1 µm size spot), notch filters to eliminate the exciter. A CCD detector with a front-illuminated open-electrode multi-pin phase, with 1024 × 256 × 16 pixels, and cooled by a Peltier system was used. Spectra were recorded in backscattering after focalization in several positions within a small

area of the sample (ca. 100 × 100 µm). The maximum laser power employed was 20 mW, and the recording time for a good signal-to-noise ratio was 10 s for 50 accumulations. LabSpec 6 was used for the spectra elaboration.

All the scanning electron microscope (SEM) experiments were conducted using a JSM-6010PLUS/LA (JEOL, Hillsboro, OR, USA) equipped with an energy-dispersive X-ray (EDX) microanalysis system (Oxford INCA-350) and field emission gun scanning electron microscope FEI Nova NanoSEM 450 FEG-SEM. All the samples were mounted on an Al stub and coated with Au using a Balzers CED-010 carbon coater (10 nm thick).

Transmission electron microscopy experiments and 3-dimensional electron diffraction (3DED) data (Gemmi et al., 2019) were collected with a JEOL JEM-F200 Multipurpose transmission electron microscopy (TEM), operating at 200 kV and equipped with a Schottky field emission gun (FEG) source. The 3DED acquisitions were performed in STEM mode after defocusing the beam to give a quasi-parallel illumination on the sample (Mugnaioli et al., 2009). A beam size of ca. 30 nm in diameter was obtained by using the highest probe size and by inserting a 10 mm condenser aperture. The 3DED data were collected in discrete steps of 1° on crystals identified by energy-dispersive X-ray spectroscopy (EDS). All data sets were performed in a range of ±30°. The camera length was 250 mm, corresponding to a resolution in direct space of ca. 0.75 Å. ED data were recorded with an ASI Cheetah hybrid pixel detector (512 × 512 pixels, 24 bit). Data were analysed by PETS2 (Palatinus et al., 2019) for cell and space group determination.

Major and minor element contents were measured by electron probe microanalysis (EPMA) at the joint laboratory (LaMA) of the DST and CNR-IGG of Florence (Italy). The instrument is a JEOL Superprobe JXA-8230, equipped with five wavelength-dispersive spectrometers operating with different diffracting crystals and detectors (gas flow and sealed Xe type). Each spectrometer holds two or four diffracting crystals with specific resolution and sensitivity, dedicated to the analysis of specific elements, including light elements, distributed as follows: spectrometer 1 holds TAPJ, LDE1, PETJ, and LDEB; spectrometer 2 holds LIFL and PETL; spectrometer 3 holds LIFH and PETH; spectrometer 4 holds LIF and PETJ; spectrometer 5 holds TAPJ and LDE2. A solid-state (SDD) energy-dispersive detector (EDS) is also present to quickly identify phases. The analytical conditions were 15 kV accelerating voltage, 10 nA beam current, and 3 µm beam diameter. A ZAF data correction model was used to get quantitative results. Counting times for major elements were 15 s on peak and 7 s for both backgrounds (apart for Na, 10 and 5 s, respectively); for minor and trace elements they were 30 s on peak and 15 s for both backgrounds. F was counted on LDE1 crystal, considering 30 s on peak and 30 s on lower background. Standardizations were performed on Astimex and Smithsonian (Fe and Ti) standards.

2.3 Milling experiments

The influence of the milling process on the morphometric characteristics of the fibrous particles/aggregates detected in the sample was investigated. To this aim, a representative batch of 400 g of the investigated clay sample was collected, quartered, and homogenized. A batch of 100 g was simply hand-ground in an agate mortar for 1 min, while three other batches of 100 g apiece underwent dry milling for 1, 5, and 10 min in a Fritsch pulverisette vibrating cup mill. In this powerful mill, milling is performed by horizontal circular oscillations of the grinding set on a vibrating plate. The grinding set consisting of ring and puck comminutes the grinding sample with extremely high pressure, impact forces, and friction. Successively, both the raw and the three batches obtained from the milling experiments were analysed with SEM described in Sect. 2.1, following the protocol reported below in Sect. 2.4.

2.4 Morphometric analysis with SEM

The raw clay sample and the three batches obtained from the milling experiments were systematically analysed with SEM (see Sect. 2.1). An amount of 5 mg of each sample was suspended in 200 m of deionized water with a 0.1 vol % surfactant additive (dioctyl sodium sulfosuccinate, $C_{20}H_{37}NaO_7S$, CAS no. 577-11-7) and kept agitated. For each sample, the same protocol was strictly applied: a volume of 1 mL of the suspension was collected at the bottom of the glass bottle containing the suspension, deposited directly on the 13 mm wide carbon adhesive film attached on an Al stub, and dried; a volume of 1 mL of the suspension was then collected at half the height of the glass bottle containing the suspension, deposited directly on carbon adhesive film attached to the Al stub, and dried; finally a volume of 1 mL of the suspension was collected at the top of the glass bottle containing the suspension, deposited directly on carbon adhesive film attached to the Al stub, and dried. In this way, comparable amounts of material were deposited for each sample. The Al stubs were all coated with Au using a carbon coater (Balzers CED-010, 10 nm thick).

For each sample, the identification and counting of the fibrous particles were obtained by secondary electron imaging, following the Italian Minister's Decree 06.09.94 (ALLEGATO II B G.U. N. 288 10/12/1994). More than 1 mm^2 of surface at 2000× magnification (400 analysis fields) was covered. EDAX point analyses for the identification of the nature of the fibres were done at 4000–10 000× magnifications. For each sample, the following parameters were measured:

- number of observed elongate mineral particles (EMPs) defined as "any mineral particle with a length (L) to width (W) ratio (aspect ratio) > 3, assuming the width of a particle to be an apparent parameter defined as the longest dimension of the particle in the plane per-

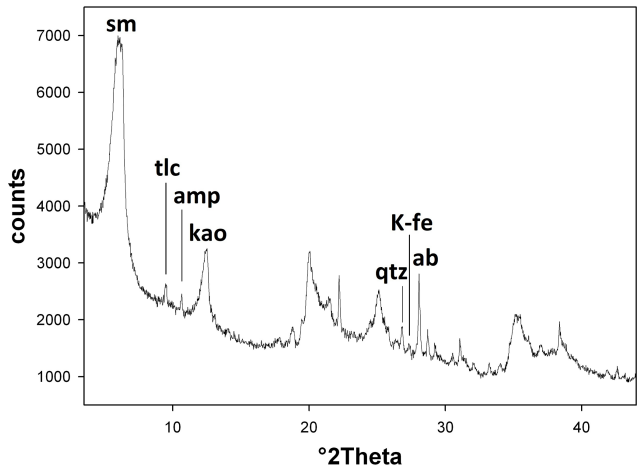

Figure 1. The X-ray powder pattern of the investigated clay sample in the range 4–43° 2θ. Legend: ab – plagioclase albite; amp – amphibole; kao – kaolinite; K-fe – potassium feldspar; qtz – quartz; sm – smectite; tlc – talc.

pendicular to length and the shortest dimension of the 2-dimensional outline of a particle" (Gualtieri et al., 2023a);

- number of observed WHO (World Health Organization) (length $L \geq 5\,\mu m$, width $W < 3\,\mu m$ and aspect ratio $L/W > 3$) fibres;
- mean L, W, and aspect ratio of the counted EMPs;
- mean L, W, and aspect ratio of the counted regulated fibres.

3 Results

The analysis of the XRPD pattern (Fig. 1) of the pale-green clay sample reveals that the major phase of the sample is a smectite (major peak at about 6.1° $2\theta = 14.5$ Å, indexed with the montmorillonite JCPDS card 00-013-059) with subordinate kaolinite (major peak at 12.4° $2\theta = 7.14$ Å; JCPDS card 01-075-0938) and plagioclase albite (major peak at 28.0° $2\theta = 3.18$ Å; JCPDS card 01-084-0982). Other minor detected phases are talc (major peak at 9.50° $2\theta = 9.30$ Å; JCPDS card 00-029-1493), amphibole (indexed as tremolite with the major peak at 10.5° $2\theta = 8.4$ Å; JCPDS card 01-085-0876), quartz (major peak at 26.6° $2\theta = 3.34$ Å; JCPDS card 01-088-2487), and K-feldspar (indexed as microcline with the major peak at 27.6° $2\theta = 3.23$ Å; JCPDS card 01-083-1604). These phases allowed the indexing of all the diffraction peaks in the powder pattern. Only the major peaks of the mineral phases are reported in Fig. 1.

The first derivative of the thermogravimetric curve (DTG, Fig. 2a and Supplement Table S1) shows nine distinct thermal events, some of which are identified by a maximum (A, B, D, E, F, H, and I) and others by shoulders (C and G). As evidenced by mass spectrometry of the emitted gases (Fig. 2b), all of these reactions involve the release of H_2O, except reactions F and G in which only CO_2 is released (reaction F) or CO_2 and H_2O are released simultaneously.

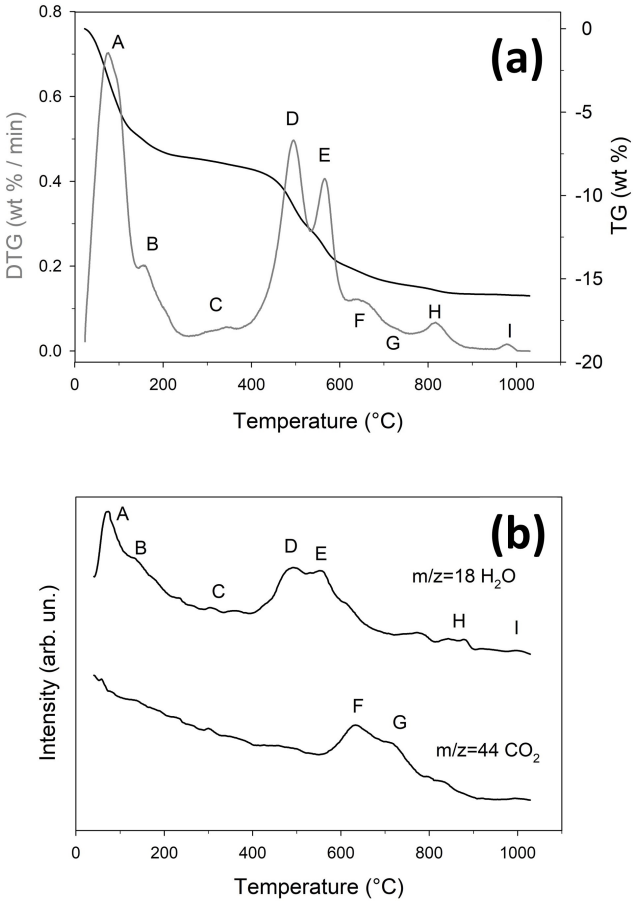

Figure 2. Thermal behaviour of the clay sample. **(a)** TG (black line) and DTG (grey line). **(b)** MSEGA curves for H_2O ($m/z = 18$) and CO_2 ($m/z = 44$); the curves for NO ($m/z = 30$) and SO_2 ($m/z = 64$) are not reported as these molecules were not detected. The slight misalignment between the DTG and MSEGA curves is due to the different heating rates (10 and 20 °C min^{-1}, respectively – see Sect. 2.2. for further details).

The thermal reactions A and B occur between 25 and 255 °C and are associated with the dehydration of smectite (Földvári, 2011), resulting in an overall mass change of 7.72 wt %; the presence of two distinct events indicates that the interlayer is predominantly occupied by a divalent cation (Guggenheim and Koster Van Groos, 2001). Reaction C, which involves a mass change of 0.49 wt %, takes place between 255 and 370 °C and is attributed to the thermal decomposition of hydroxides not detectable through XRPD. Reactions D and E, partly overlapping, occur between 370 and 615 °C and are attributed to the dehydroxylation of kaolinite and smectite, respectively (Földvári, 2011; Guggenheim

and Koster Van Groos, 2001), resulting in an overall mass change of 6.08 wt %. Reactions F (partly overlapping with E) and G occur between 615 and 750 °C, leading to a total mass change of 1.08 wt %; considering that CO_2 release occurs in two steps (Fig. 2b), these reactions could be attributed to the thermal decomposition of dolomite or calcite and dolomite (Bloise et al., 2016; Mackenzie, 1970; Malferrari et al., 2021; Taufiq-Yap et al., 2014), again not observable by XRPD. Thermal reaction G is also associated with H_2O release due to an initial dehydroxylation reaction of tremolite (Apollaro et al., 2018; Bloise et al., 2008). Reactions H (765–895 °C, 0.48 wt %) and I (950–1000 °C, 0.047 wt %) are attributed to the dehydroxylation of talc (L'vov and Ugolkov, 2005; Wesołowski, 1984) and tremolite (Bloise, 2023; Bloise et al., 2017), respectively, with the latter forming meta-tremolite (Gualtieri and Tartaglia, 2000).

The micro-Raman experiments were conducted on 30 different particles: 23 particles displayed a pattern like the one shown in Fig. 3a; 5 particles displayed a pattern like the one shown in Fig. 3b; 2 particles displayed a pattern like the one shown in Fig. 3c. The analysis of the spectra allowed us to identify an amphibole phase, presumably tremolite, for the family of spectra equivalent to that in Fig. 3a and b. The observed bands are interpreted as follows: 61, 115–119, 172–175, and 217–225 cm^{-1} as lattice vibrations; 296–297, 364, 387–389, 408–409, and 524–528 cm^{-1} as Mg–OH and Fe–OH vibrations, Si–O–Si bending motions, and OH librations; 668–670 and 737–739 cm^{-1} as strong Si–O–Si symmetric stretching; 926–929, 1026–1027, and 1059–1064 cm^{-1} as O–Si–O symmetric stretching and the O–Si–O and Si–O–Si asymmetric stretching motions (Bersani et al., 2019; Rinaudo and Croce, 2019). The two spectra equivalent to that in Fig. 3c have been identified as a pyroxene phase. The observed bands are interpreted as follows: 132, 192, 222, and 240 cm^{-1} as lattice vibrations; 320, 355, 387, 421, and 463 cm^{-1} as non-tetrahedral cation vs. oxygen stretching of M1–O and M2–O bonds (Huang et al., 2000; Tribaudino et al., 2012); 505, 552, 662, 702, and 748 cm^{-1} as chain bending and/or stretching (Wang et al., 2001; Tribaudino et al., 2012); 790, 851, and 906 cm^{-1} as T–O stretching peaks; 1008 cm^{-1} as stretching modes of Si and non-bridging oxygen atoms within the SiO_4 tetrahedron (Wang et al., 2001; Tribaudino et al., 2012); and 1104 cm^{-1} as O–Si–O symmetric stretching and the O–Si–O and Si–O–Si asymmetric stretching motions.

Figure 4 shows a selection of SEM pictures of various elongated amphibole particles detected in the clay sample. Specifically, we observed compact fibre bundles (Fig. 4a), cleavage fragments (Fig. 4b), EMPs (Fig. 4c), and fibrous particles or asbestiform fibres (Fig. 4d). The relative EDS point analyses (Supplement Fig. S1) invariably point to a tremolite composition with Si, Ca, and minor Fe and Al. In the sample we also observed EMPs of various nature. Figures S2 and S3 report a selection of these particles with the relative EDS point analyses. Specifically, an acicular particle with a composition compatible with that of a mica is portrayed in (a); clay mineral particles in (b), (c), and (f); a titanium oxide in (d); and cristobalite or quartz in (e).

The TEM study allowed us to confirm the identification of three different families of elongated crystals. Figure 5 reports a selection of crystals representative of the three families with an example of nano-beam electron diffraction (NED) pattern and relative EDS spot analysis. For each crystal, 61 patterns (from −30 to +30°) were collected and used for cell determination. The indexing of the tremolite crystal reported in Fig. 5a yielded the following monoclinic unit cell parameters: $a = 9.83(3)$ Å, $b = 18.21(4)$ Å, $c = 5.29(3)$ Å, and $\beta = 104.34(8)°$. The indexing of the Al-rich tremolite crystal reported in Fig. 5b yielded the following monoclinic unit cell parameters: $a = 9.86(4)$ Å, $b = 18.18(4)$ Å, $c = 5.30(3)$ Å, and $\beta = 104.93(9)°$. These parameters are in line with the unit cell parameters reported in literature for fibrous tremolite samples (see, for example, Verkouteren and Wylie, 2000). The indexing of the pyroxene crystal reported in Fig. 5c allowed us to calculate the following monoclinic unit cell parameters: $a = 9.82(3)$ Å, $b = 8.98(5)$ Å, $c = 5.26(4)$ Å, and $\beta = 105.71(7)°$. These parameters are compatible with the unit cell parameters reported in literature for diopside (see, for example, Rutstein and Yund, 1969; Thompson and Downs, 2008).

Figure 6 shows an example of an EDS map collected in STEM mode from a fibrous tremolite aggregate. The distribution of Al clearly shows that Al-rich and Al-poor fibres are intergrown within the same aggregate.

The EPMAs were conducted on a statistically significant number of crystals representative of the three families of EMPs present in the sample: Al-rich and Al-poor tremolites crystals intimately interdispersed (Fig. 7a) and elongated particles of pyroxene crystals (Fig. 7b). All the collected point analyses are reported in Table S2 of this paper. Several outliers, likely due to contamination of clay phases, were removed, and the chemical formula of the three phases was calculated on the basis of 23 oxygens for the amphibole (tremolite) and 6 oxygens for pyroxene (diopside). The calculated chemical formulae are given below.

- $Na_{0.08}(Ca_{1.73}Fe_{0.256}Na_{0.015})_{2.00}(Mg_{4.474}Al_{0.166}Fe_{0.353}Mn_{0.007})_{5.00}(Si_{7.756}Al_{0.234}Ti_{0.01})_{8.00}O_{22}(OH)_2$ for Al-rich tremolite
- $(Ca_{1.86}Fe_{0.096}Na_{0.045})_{2.001}(Mg_{4.5}Al_{0.095}Fe_{0.395}Mn_{0.01})_{5.00}(Si_{7.945}Al_{0.05}Ti_{0.005})_{8.00}O_{22}(OH)_2$ for tremolite
- $(Ca_{0.868}Fe_{0.111}Na_{0.022})(Mg_{0.856}Al_{0.075}Fe_{0.065}Mn_{0.004})(Si_{1.935}Al_{0.055}Ti_{0.01})O_6$ for diopside.

The statistics of the particles counted from the SEM quantitative analysis of the samples obtained from the milling experiments (number of observed EMPs, number of observed WHO fibres, and their mean length L, width W, and aspect

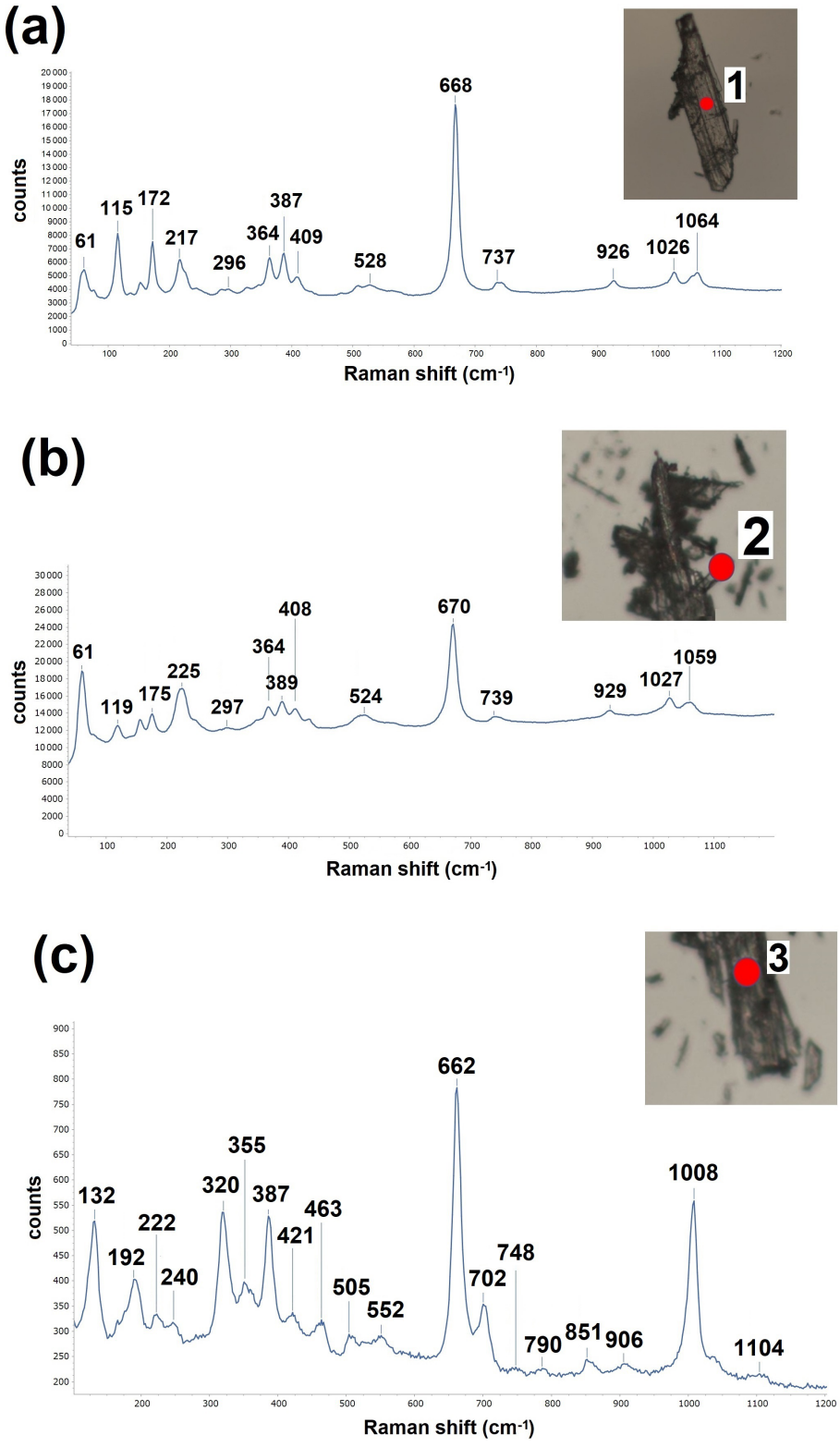

Figure 3. A selection of micro-Raman representative patterns conducted on 30 different EMPs of the sample. **(a)** The trace displayed by 23 particles, **(b)** the trace observed for 5 particles, and **(c)** the trace observed for 2 particles.

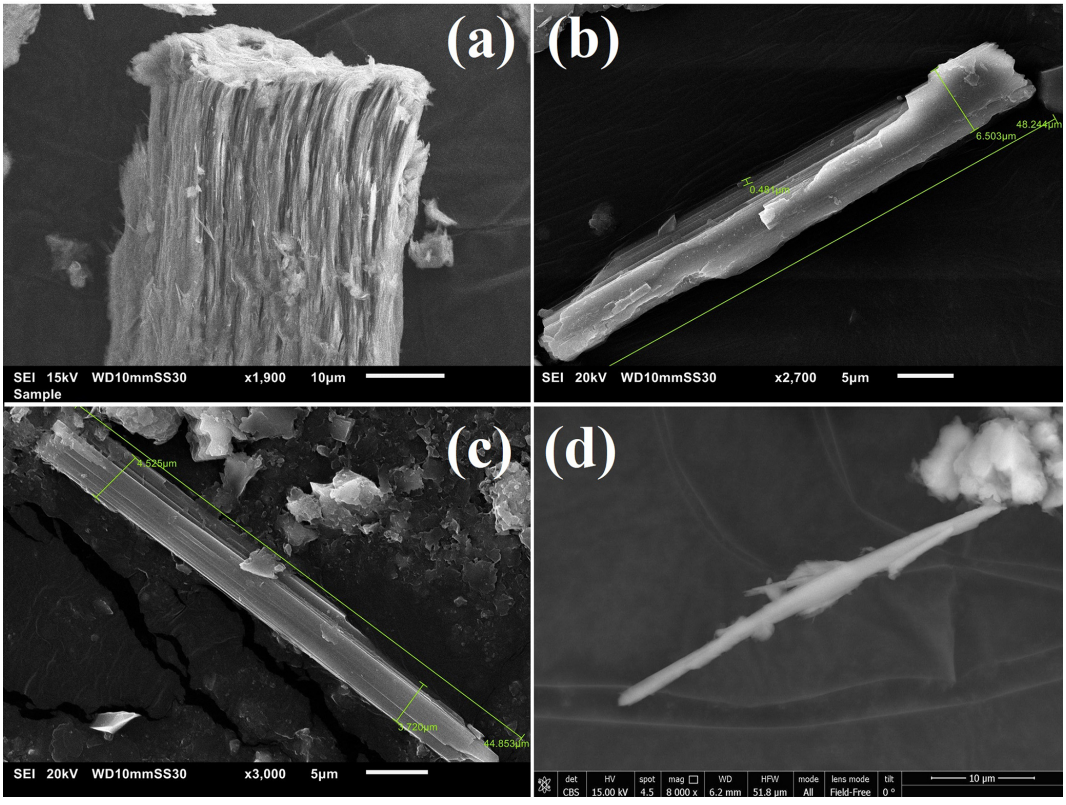

Figure 4. Gallery of SEM images of various elongated amphibole particles observed in the investigated clay sample: **(a)** compact fibre bundle, **(b)** cleavage fragments, **(c)** EMP, and **(d)** fibrous asbestiform shape. All the particles have been identified as tremolite (the relative EDS point analyses have been provided as Supplement S1).

ratio L/W) are reported in Table 1. All the measured data are available upon request to the corresponding author.

4 Discussion

4.1 Identification of the mineral fibres

In this study, we detected the presence of asbestos fibres (amphibole asbestos biodurable fibres: Gualtieri et al., 2018b) in a plastic clay sourced from the mining district of Gomsiqe–Puka in Albania, commonly utilized in the production of traditional ceramics. This material originates from the green layers within a clay deposit associated with altered gabbros and basalts of the ophiolitic Mirdita (Saccani and Tassinari, 2015; Nicolas et al., 2017). The primary newly formed phases observed are smectite and kaolinite, while the predominant residual phase inherited from the original gabbroic rock is plagioclase. Additionally, minor residual phases identified include talc, quartz, alkaline feldspar, and amphibole.

Tremolite–actinolite formation by oceanic hydrothermal alteration of clinopyroxene and/or olivine in gabbroic rocks is a common process in the oceanic crust (e.g. Cannat et al., 1992; Nozaka and Fryer, 2011). However, tremolite could also form in these rocks during obduction processes (e.g. Zhao et al., 2021; Ábalos et al., 2022).

Our findings corroborate the assertion made by Gualtieri et al. (2023b) that only a multidisciplinary approach ensures the unequivocal identification of asbestos fibres in complex natural materials such as the one examined here. As mentioned earlier, XRPD and thermal analysis traces (Figs. 1 and 2) indicated the presence of an amphibole phase but provided no insight into its crystal morphology, a crucial factor for discriminating between asbestos and non-asbestos particles. Conversely, micro-Raman spectroscopy and electron microscopy techniques revealed the fibrous nature of the particles and facilitated their mineralogical and chemical identification. TEM with relative EDS analyses and 3DED once again were demonstrated to be powerful techniques for identifying and characterizing mineral fibres at the nanoscale using very small amounts of sample. The only disadvantage is that these experimental methods are quite expensive and time-consuming.

Three different types of EMPs were identified. Most of them are classified as Al-rich tremolite and tremolite; a very minor amount of EMP is instead classified as diopside. Apparently, the Na and Al contents do not rule the crystal

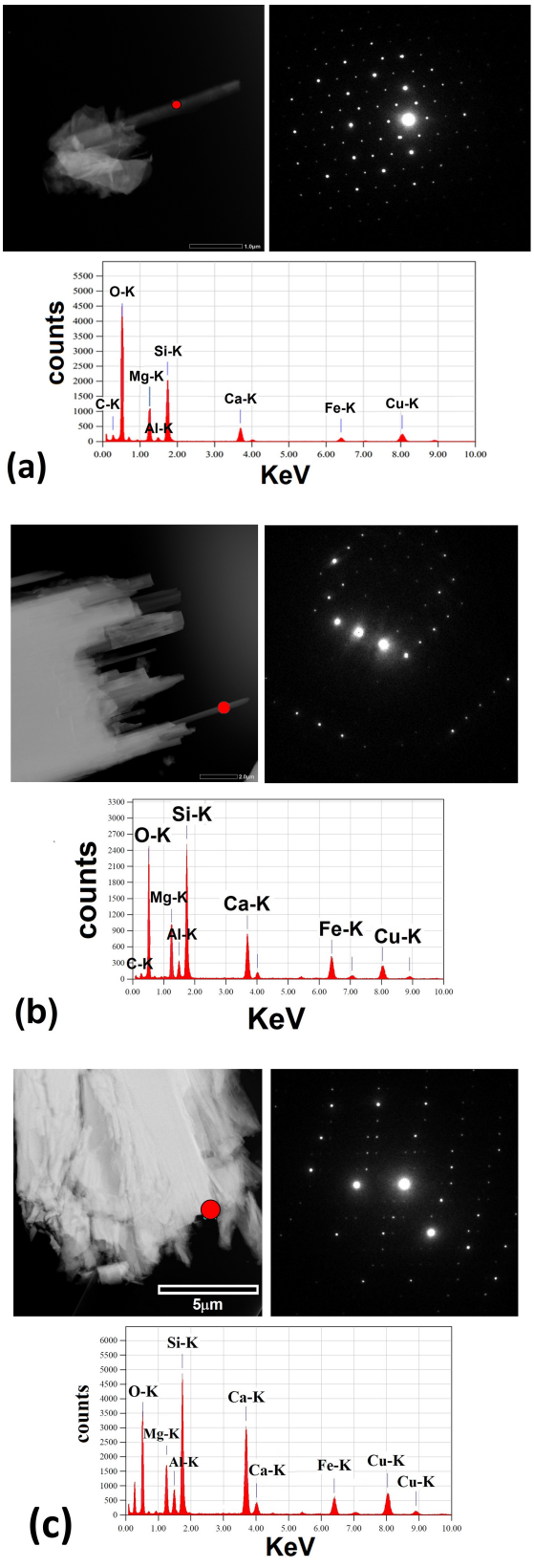

Figure 5. Selection of the results of the TEM experiments. STEM images, nano-beam electron diffraction, and EDS spots analysis of **(a)** tremolite crystals, **(b)** Al-rich tremolite crystals, and **(c)** pyroxene crystals. The red circle indicates the approximate area of the analysis.

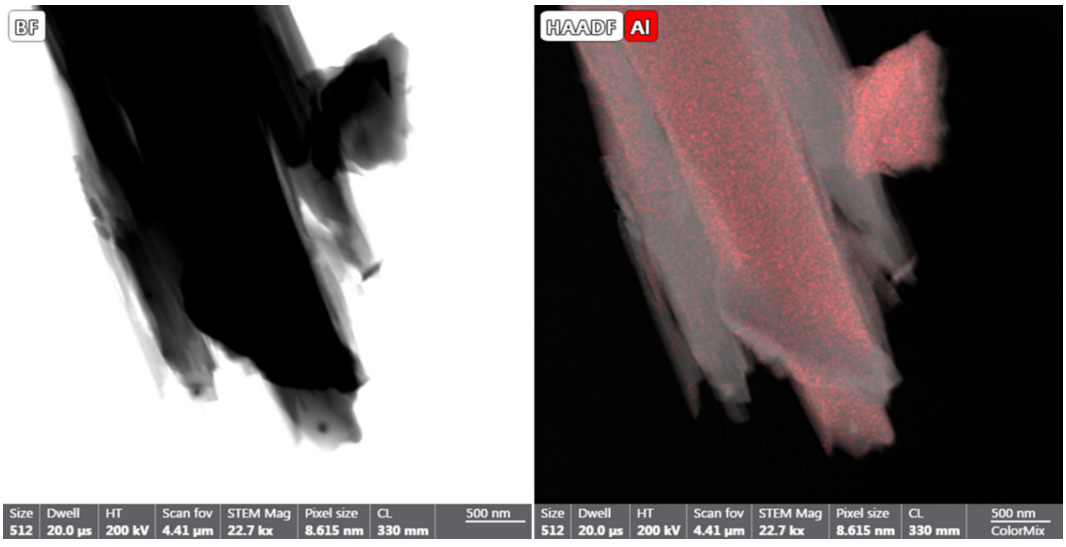

Figure 6. Aluminium map collected with EDS in STEM mode from a fibrous tremolite aggregate. The map shows that Al-rich fibres are intergrown with Al-poor fibres.

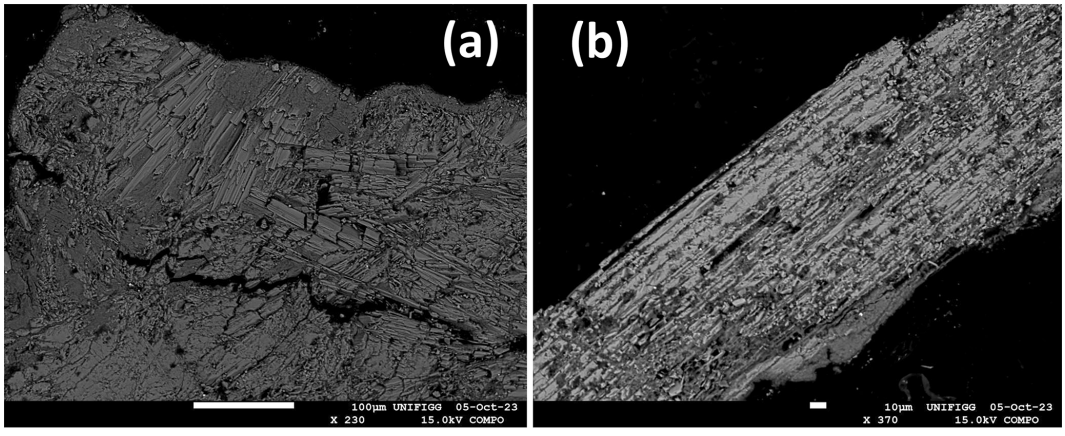

Figure 7. Example of grains analysed with EPMA: **(a)** aggregates of Al-rich and Al-poor tremolite crystals intimately interdispersed and **(b)** aggregates of elongated particles of pyroxene crystals.

growth and crystal shape, as both the Al-rich and Al-poor terms are fibrous with particles classified as asbestos.

Compositionally, the Al-rich tremolite is similar to other tremolites found in oceanic settings (Table 2), showing higher Al, Fe, and alkali content with respect to the Al-poor term, which is instead more similar to continental tremolites being enriched in Si and Ca and close to the end-member composition of tremolite (Fig. 8). It is well known that Al content in calcium amphibole is dependent on T and P (e.g. Ernst and Liu, 1998), which are commonly higher in an oceanic hydrothermal flux with respect to obduction processes, while Di Giuseppe et al. (2021) suggested that Na content in tremolites depends on Al exchanges. They also show that oceanic and continental tremolites plot on divergence Fe–Si and Mg–Si trends and that, in several cases, ophiolitic tremolites follow the continental trend, being formed during obduction processes (Fig. 8; Di Giuseppe et al., 2021). The finding of two different tremolite terms entangled at the nano-scale in the same lithology (Fig. 6) suggests that tremolite from the mining district of Gomsiqe–Puka was originally formed in oceanic conditions (Al-rich term) and partially modified during the obduction process up to the Al-poor term by loss of Al, Fe, and Na in favour of Si and Ca. These elements could be easily provided at the percolating fluids by plagioclase and/or carbonates, with the first present in the rock protolith and the second occurring today in the mineralogical association (and thus possibly precipitated from the percolating fluids or already occurring in the protolith).

Fibrous diopside is a rare occurrence in nature. Its presence in various geological settings has been sporadically documented (see, for instance, Belluso and Ferraris, 1991; Stripp

Table 1. Number and morphometric parameters of the fibrous particles counted from the SEM quantitative analysis of the samples obtained from the milling experiments. Standard deviations are in parentheses.

Milling time (min)	0	1	5	10
No. EMP	6(1)	2(1)	1	1
No. WHO fibres	2(2)	9(6)	9(0.7)	3(2)
Mean L EMP	29(41)	17.8(7.4)	15.2	11.5
Mean W EMP	7(13)	4.6(2.1)	5.9	3.9
Mean L/W EMP	4.7(5.4)	3.93(0.14)	3.8	3.02
Mean L WHO fibres	11	8.48(2.6)	8.19(4.3)	9.07(3.6)
Mean W WHO fibres	0.9(0.1)	1(0.3)	1.38(0.8)	1.21(0.9)
Mean L/W WHO fibres	12.4(1.9)	10(6.5)	7.18(4.7)	10.51(8.9)
C of WHO fibres (ppm/wt %)	250/0.025	1070/0.107	1968/0.1968	558/0.0558

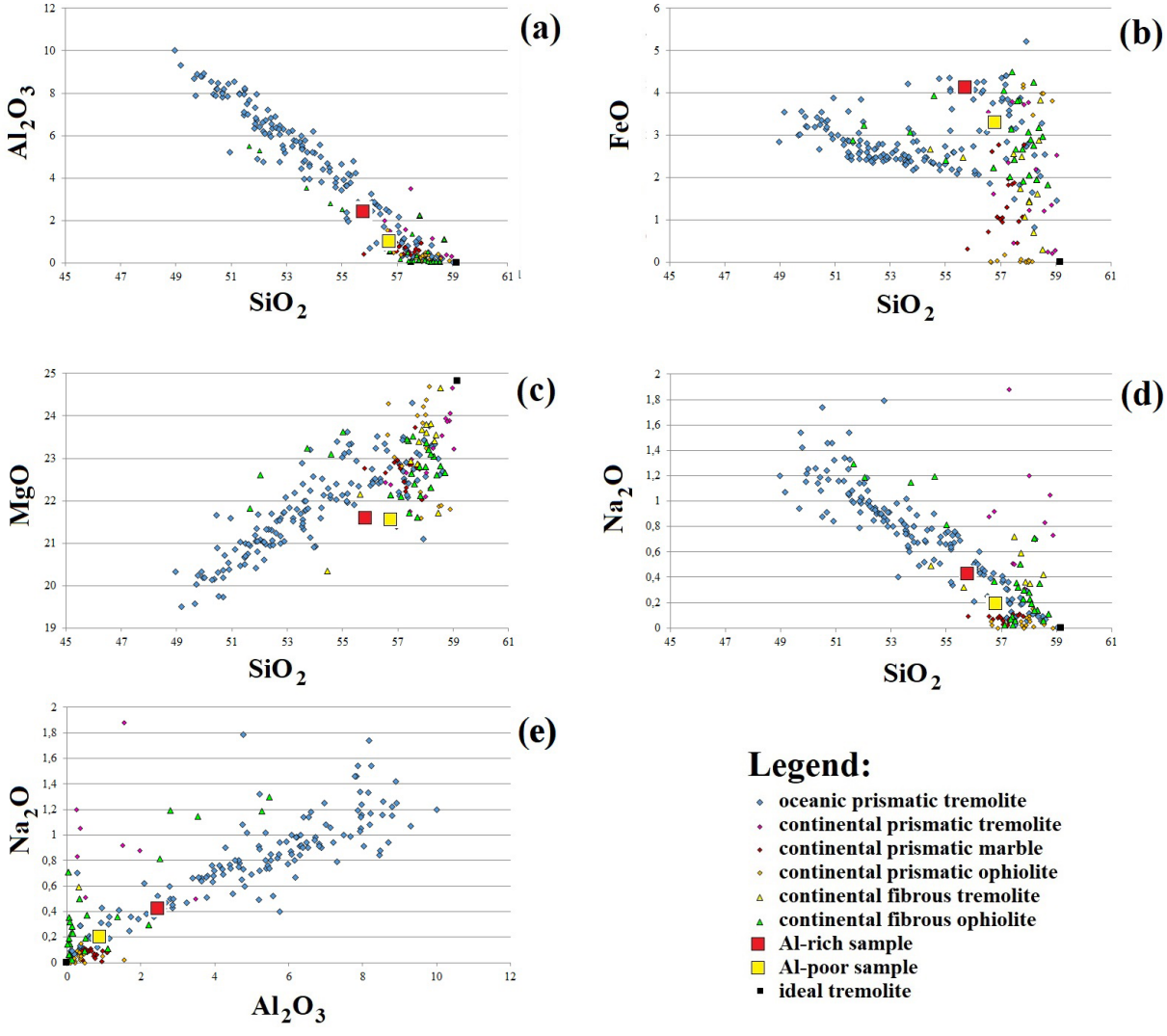

Figure 8. Comparison between the composition of the major elements of the investigated tremolites and that of tremolite amphiboles from oceanic and continental tectonic environments. Crossplot of **(a)** Al_2O_3 (wt %) versus SiO_2 (wt %), **(b)** FeO (wt %) versus SiO_2 (wt %), **(c)** MgO (wt %) versus SiO_2 (wt %), **(d)** Na_2O (wt %) versus SiO_2 (wt %), and **(e)** Na_2O (wt %) versus Al_2O_3 (wt %). The $\pm 1\sigma$ compositional variability of the samples is within the symbol area (see text for details).

Table 2. Comparison of the chemistry of our samples with that of fibrous tremolites of different origin and with different Al content, in decreasing order (see text for details).

Sample	Structure site assignment*			
	A	B	C	T
Al-rich sample	$Na_{0.08}$	$Ca_{1.73}Fe_{0.256}Na_{0.015}$	$Mg_{4.474}Al_{0.166}Fe_{0.353}Mn_{0.007}$	$Si_{7.756}Al_{0.234}Ti_{0.01}$
Al-poor sample	–	$Ca_{1.86}Fe_{0.096}Na_{0.045}$	$Mg_{4.5}Al_{0.095}Fe_{0.395}Mn_{0.01}$	$Si_{7.945}Al_{0.05}Ti_{0.005}$
Mid-Atlantic Ridge	$Na_{0.29}$	$Ca_{1.92}Fe_{0.08}$	$Mg_{4.80}Fe_{0.20}$	$Si_{7.52}Al_{0.48}$
Leka Ophiolite Complex (Norway)	$K_{0.01}Na_{0.18}$	$Ca_{1.76}Na_{0.34}$	$Mg_{4.50}Fe^{2+}_{0.37}Fe^{3+}_{0.02}Mn_{0.02}Ni_{0.01}Cr_{0.06}$	$Si_{7.755}Al_{0.30}$
Gouverneur Mining District (NY, USA)	$K_{0.12}Na_{0.18}$	$Ca_{1.8}Na_{0.20}$	$Mg_{4.94}Fe_{0.06}$	$Si_{7.80}Al_{0.20}$
Kallidromon (central Greece)	–	$Ca_{1.789}Fe^{2+}_{0.139}Mg_{0.07}$	$Mg_{4.799}Fe^{2+}_{0.025}Fe^{3+}_{0.017}Al_{0.046}$	$Si_{7.954}Al_{0.138}$
Çankırı/Ankara (central Anatolia, Türkiye)	$Na_{0.17}K_{0.07}$	$Ca_{1.59}Mg_{0.19}Mn_{0.002}$	$Mg_{4.72}Fe_{0.28}$	$Si_{7.86}Al_{0.1}Fe_{0.06}$
Virtasalmi (Finland)	–	$Ca_{1.96}Na_{0.01}$	$Mg_{5.03}Fe_{0.03}$	$Si_{7.98}Al_{0.02}$
Susa Valley (Piedmont, Italy)	–	$Ca_{1.95}Na_{0.05}K_{0.01}$	$Mg_{4.84}Al_{0.01}Fe^{2+}_{0.11}Fe^{3+}_{0.02}Mn_{0.02}$	Si_8
Lanzo Valleys (Piedmont, Italy)	–	$Ca_{1.96}Na_{0.01}K_{0.01}$	$Mg_{4.69}Fe^{2+}_{0.26}Fe^{3+}_{0.03}Mn_{0.03}$	Si_8

Sample	Genetic environment	Reference
Al-rich sample	?	This study
Al-poor sample	?	This study
Mid-Atlantic Ridge	Oceanic floor serpentinization	Di Giuseppe et al. (2021)
Leka Ophiolite Complex (Norway)	Oceanic floor serpentinization	Iyer et al. (2008)
Gouverneur Mining District (NY, USA)	Contact regional serpentinization	Hawthorne and Grundy (1976)
Kallidromon (central Greece)	Orogenetic subduction serpentinization of marginal oceanic floor	Karipi et al. (2006)
Çankırı/Ankara (central Anatolia, Türkiye)	Oceanic floor tectonically controlled hydrothermal serpentinization	Külah et al. (2018)
Virtasalmi (Finland)	Skarn continental regional metamorphism	Hytönen and Ojanperä (1976)
Susa Valley (Piedmont, Italy)	Orogenetic subduction metamorphism	Ballirano et al. (2008)
Lanzo Valleys (Piedmont, Italy)	Continental orogenetic subduction metamorphism	Pacella et al. (2008)

* Assuming the ideal formula $AB_2C_5T_8O_{22}(OH)_2$.

et al., 2006) or noted as exceptional, as seen in the case of fibrous diopside inclusions found in demantoid garnet gems from the Urals (Russia) (Krzemnicki, 1999). This marks the first instance of observing and quantifying diopside EMPs as dust contaminants in a natural material. It is worth noting that diopside is neither classified nor regulated and poses no health hazard.

It is crucial to emphasize that only a thorough investigation using electron microprobe analysis enabled the discrimination of elongated diopside particles from elongated tremolite

particles. Although diopside EMPs are present here in very low concentrations, they could be confused for tremolite during the quantitative SEM analysis. It is plausible to assume that in other scientific or analytical case studies, fibrous diopside may have been mistakenly identified as fibrous tremolite.

4.2 How milling affects identification and quantification of the mineral fibres

The comprehensive investigation into the impact of the milling process on both the identification and quantification of asbestos tremolite fibres has provided some insights. Table 1 and Fig. 9 present informative trends regarding the number of counted particles and their size concerning milling time, affirming the liberation of individual countable fibres from cleavage fragments, and bundles during milling. Indeed, there is a trend of a decrease in the number of tremolite EMPs and elongated particles with increasing milling time from 0 to 10 min (Fig. 9a and Table 1), while the coarser aggregates release smaller WHO fibres, whose count increases with milling times of 1 and 5 min, with the exception of the point at 10 min. Correspondingly, the mean length (L) and width (W) of observed EMPs tend to decrease with increasing milling time from 0 to 10 min (Fig. 9b, c and Table 1). The mean length L of the WHO fibres also exhibits a decreasing trend with increasing milling times of 1 and 5 min (Fig. 9b and Table 1), with the exception of the point after 10 min (see the explanation below). The mean width W of the WHO fibres experiences a slight increase due to the separation of coarse aggregates and bundles, resulting in thicker regulated fibres, with increasing milling times (Fig. 9c and Table 1).

Our findings align with previous literature data. Wylie and Schweitzer (1982) demonstrated that longer grinding times produce less elongated wollastonite particles with lower aspect ratio. Schneider et al. (1998), using optical microscopy, reported a decrease in length and diameter of tremolite fibres in acid-washed dolomite and talc with milling times ranging from 0 to 15 min. Baietto (2019) observed that tremolite particles, initially fibrous in appearance, exhibited reduced fibrosity after grinding as prismatic elements became dominant.

Particular attention should be paid to samples subjected to longer milling times (10 min), where overgrinding results in fibre breakdown, leading to a decrease in the number of counted WHO fibres with lengths exceeding 5 µm (Fig. 9 and Table 1). This finding also concurs with existing literature. Bloise et al. (2018b) noted that for extended milling times, the lengths of asbestos amphiboles decrease and should fall below the WHO limit of 5 µm, underscoring the significant impact of milling time on the quantification of respirable fibres in the sample.

Our results reveal that sample comminution affects both the identification and quantification of tremolite asbestos in

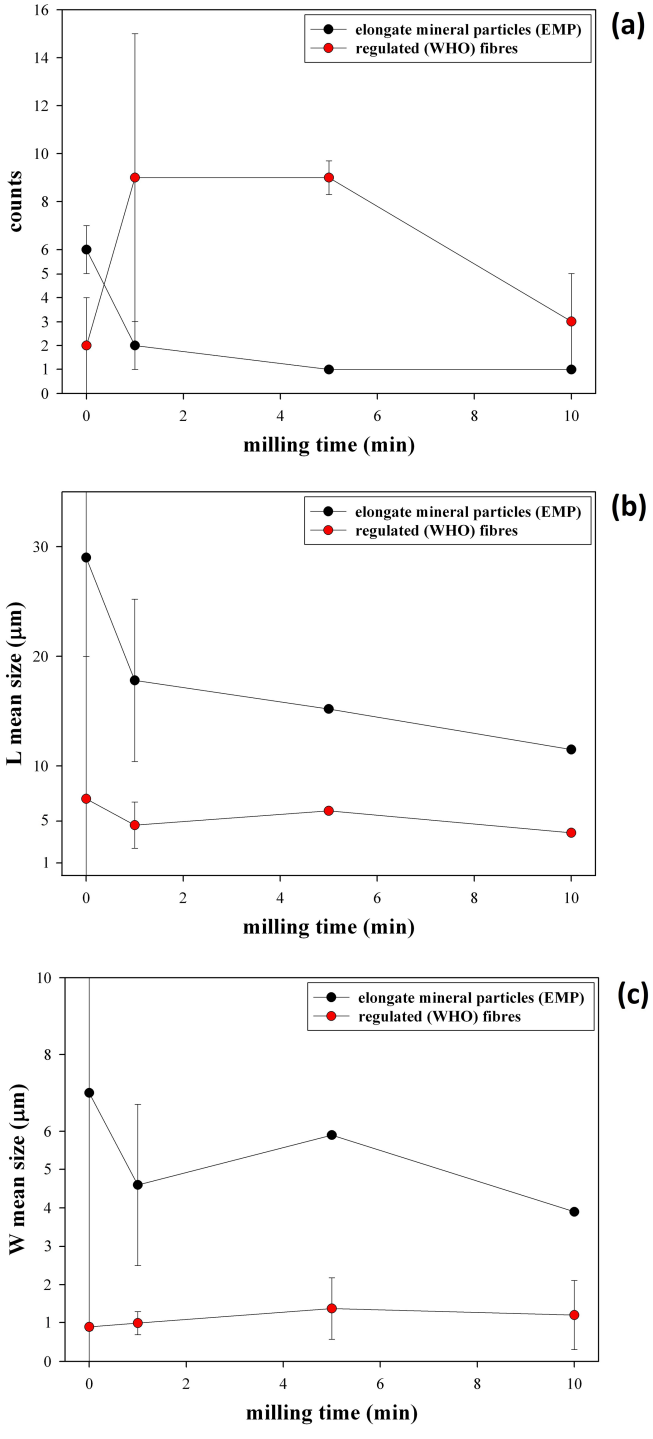

Figure 9. Statistics of the particles counted from the SEM quantitative analysis vs. milling time: **(a)** plot of the number of observed EMPs and WHO fibres, **(b)** plot of the mean length L of the observed EMPs and WHO fibres, and **(c)** plot of the mean width W of the observed EMPs and WHO fibres.

the sample, thereby influencing its classification as asbestos-containing or asbestos-free material.

Towards an effective global harmonization system (GHS), the European Union REACH compliance prohibits any intentional use of asbestos, but allows the presence of category 1A carcinogens, including asbestos, as contaminant in concentrations < 0.1 wt % without obligation of labelling. The REACH compliance is conflicting with more severe domestic laws of some parties that apply "zero tolerance" for asbestos like France, Germany, and Italy. In these countries, the presence of asbestos, irrespective of its concentration, is adequate to classify a material as asbestos-contaminated and declare it illicit (Décret 96-1133, 1996; Gesetz 162, 1993; Italian Law 257, 1992). As per domestic legislation, assessment of asbestos presence is confirmed when a single particle observed with SEM displays the chemical composition of one of the six asbestos species and meets regulated dimensions ($L \geq 5$ µm, $W \leqq 3$ µm, and $L/W \geqq 3$). Milling increases the number of regulated fibres, thereby enhancing the likelihood of identifying an asbestos fibre. While the probability of asbestos fibres' presence in the raw sample is minimal, it increases in samples milled for 1 and 5 min before drastically decreasing under overmilling conditions (10 min).

As said, European Union REACH compliance (EC 2006/1907, 2006) permits the unintentional presence of asbestos in a commercial product in concentrations < 0.1 wt % without obligatory labelling. Consequently, precise asbestos quantification is vital and potentially influenced by comminution. In this specific case, we followed the protocol for asbestos quantification in massive materials using SEM, as outlined by Italian legislation (Italian Ministry of Health, 1994), which is akin to the International Standard Organization (ISO) Methods 14966 (ISO, 2019) and 22262-1 (ISO, 2012). Concentration (C) of asbestos fibres (in ppm) can be calculated using the following equation:

$$C = [(A \cdot w_a)/(n \cdot a \cdot W)] \cdot 10^6,$$

where A = filter surface (mm^2) = 132.73 mm^2; w_a = total weight of counted tremolite asbestos fibres (mg) assuming that the volume of a single fibre is approximated to that of a cylinder, and the weight is calculated assuming an average density of tremolite of 3050 mg cm^{-3}; n = number of analysed fields = 400; a = field surface (mm^2) = 0.003149 mm^2; W = weight of the sample on the filter (mg) = 0.018 mg. The last line of Table 1 reports the concentration C calculated for the regulated (asbestos) fibres in the raw and milled samples. The calculations demonstrate that milling alters the classification of the raw material: the raw sample is within the limits of the REACH compliance (< 0.1 wt %) and marketable, while the samples milled for 1 and 5 min result illegal as asbestos concentration is > 0.1 wt %. Overmilling (10 min) brings back the concentration of asbestos in the sample to values < 0.1 wt % and marketable.

5 Conclusions

In this study, we conducted a comprehensive characterization of a clay sourced from the green horizon of the mining area of Gomsiqe–Puka in Albania. We aimed to highlight the challenges associated with detecting the presence of asbestos, especially when it occurs at concentrations near the detection limit. Accurate identification and quantification of asbestos fibres are crucial for correctly classifying and regulate these materials.

Our analysis revealed that the clay primarily comprises newly formed smectite and kaolinite, alongside residual plagioclase. Additionally, minor phases such as talc, quartz, alkaline feldspar, and amphibole were detected. Our focus was on the minor amphibole phase to determine whether its shape was fibrous asbestiform. Through electron microscopy and EPMA techniques, we unequivocally identified three distinct types of amphibole-like EMPs. The majority were classified as Al-rich tremolite and tremolite, while the third type was identified as pyroxene (diopside). Notably, this marks the first observation and measurement of dust-contaminating natural materials containing fibrous diopside, which, unlike amphibole asbestos, is not classified or regulated as hazardous.

The Al-rich tremolite identified here is similar to tremolites found in oceanic settings, with higher Al, Fe, and alkali content with respect to the Al-poor term, which is more similar to continental tremolites enriched in Si and Ca and close to the tremolite end-member composition.

Our systematic investigation into the influence of milling processes on the identification and quantification of asbestos tremolite fibres revealed significant findings. We observed that the number of tremolite EMPs, cleavage fragments, and elongated particles decreased with milling times (1–5 min), with smaller WHO fibres emerging. However, prolonged milling (10 min) resulted in overgrinding, leading to a decrease in the number of counted WHO fibres with lengths exceeding 5 µm. Thus, our results indicate that sample comminution affects both the analytical identification and quantification of amphibole asbestos, consequently impacting its classification as a hazardous or non-hazardous material. The raw sample appeared to comply with REACH directive limits as far as the permissible concentration of carcinogens (< 0.1 wt %) is concerned. On the other hand, the samples milled for 1 and 5 min exceeded the permissible asbestos concentration, whereas overmilling (10 min) again reduced the asbestos concentration to below 0.1 wt %.

These results raise a fundamental question: should samples be ground for regulated asbestos fibre analysis and counting in massive materials? The Italian Decree 06/09/94 recommends comminution before sample preparation but acknowledges its approximate nature and the physical changes induced in the sample. Nonetheless, comminution mimics common manufacturing and wear processes, enabling a more accurate assessment of potential exposure risks under critical

operational conditions. Particularly, considering the intended use of the clay in ceramic formulations, which involves wet milling during the ceramic process, controlled milling of the sample before asbestos fibre identification and quantitative determination seems justified.

Data availability. All data reported in this article are available upon request to the corresponding author.

Supplement. The supplement related to this article is available online at: https://doi.org/10.5194/ejm-36-749-2024-supplement.

Author contributions. AFG: writing – original draft, supervision, methodology, analysis, data curation, conceptualization, editing, review. SMD: analysis. DM: analysis, writing, editing, review. TG: analysis, editing, review. RF: analysis, writing, editing, review. MS: analysis. RA: analysis. MCG: analysis, review. EB: analysis, review. AO: analysis, review. EM: analysis, writing, editing, review.

Competing interests. At least one of the co-authors is a member of the editorial board of *European Journal of Mineralogy*. The peer-review process was guided by an independent editor, and the authors also have no other competing interests to declare.

Disclaimer. Publisher's note: Copernicus Publications remains neutral with regard to jurisdictional claims made in the text, published maps, institutional affiliations, or any other geographical representation in this paper. While Copernicus Publications makes every effort to include appropriate place names, the final responsibility lies with the authors.

Special issue statement. This article is part of the special issue "Celebrating the outstanding contribution of Paola Bonazzi to mineralogy". It is not associated with a conference.

Acknowledgements. Part of this work was the project of the bachelor's thesis of Gian Marco Barbieri. Domenico Barani (Lasselsberger Group GmbH) is kindly acknowledged for providing the samples for the study. TEM analyses were supported by the Centre for Instrument Sharing of the University of Pisa (CISUP). The associate editor and the two referees are kindly acknowledged for the constructive revision of the manuscript.

Financial support. This research has been supported by the MUR – PRIN2022 programme under the project "SEEDS – Sediments Eco-recycling Exploitation, Development and Sustainability" (grant agreement no. 2022BCL34N).

Review statement. This paper was edited by Marco Pasero and reviewed by two anonymous referees.

References

Ábalos, B., Puelles, P., and Ibarguchi, J. I. G.: Polyphase tectonic reworking of serpentinites and chlorite-tremolite-talc rocks (SW Spain) from the subduction forearc to intracontinental emplacement, J. Metamorph. Geol., 41, 491–523, 2022.

Apollaro, C., Fuoco, I., Vespasiano, G., De Rosa, R., Cofone, F., Miriello, D., and Bloise, A.: Geochemical and mineralogical characterization of tremolite asbestos contained in the Gimigliano-Mount Reventino Unit (Calabria, south Italy), J. Mediterranean Earth Sci., 10, 5–15, 2018.

Baietto, O.: Naturally Occurring Asbestos: the problem of quantification. Doctoral Dissertation Doctoral Program in Energy Engineering (31st Cycle), University of Torino, Italy, 2019.

Baietto, O., Diano, M., Zanetti, G., and Marini, P.: Grinding test on tremolite with fibrous and prismatic habit, Fibers, 7, 52, https://doi.org/10.3390/fib7060052, 2019.

Ballirano, P., Andreozzi, G. B., and Belardi, G.: Crystal chemical and structural characterization of fibrous tremolite from Susa Valley, Italy, with comments on potential harmful effects on human health, Am. Mineral., 93, 1349–1355, 2008.

Belardi, G., Vignaroli, G., Trapasso, F., Pacella, A., and Passeri, D.: Detecting asbestos fibres and cleavage fragments produced after mechanical tests on ophiolite rocks. Clues for the asbestos hazard evaluation, J. Mediterranean Earth Sci., 10, 63–78, 2018.

Belluso, E. and Ferraris, G.: New data on balangeroite and carlosturanite from alpine serpentinites, Eur. J. Mineral., 3, 559–566, 1991.

Berman, D. W. and Kolk, A. J.: EPA 540-R-97–028 Superfund Method for the Determination of Asbestos in Soils and Bulk Materials, Prepared for the Office of Solid Waste and Emergency Response, U.S. Environmental Protection Agency, 1997.

Bersani, D., Andò, S., Scrocco, L., Gentile, P., Salvioli-Mariani, E., Fornasini, L., and Lottici, P. P.: Composition of amphiboles in the tremolite–ferro–actinolite series by Raman Spectroscopy, Minerals, 9, 491, https://doi.org/10.3390/min9080491, 2019.

Bloise, A.: On the thermal breakdown of tremolite: a new method for distinguishing between asbestos and non-asbestos tremolite samples, J. Mater. Sci., 58, 8779–8795, 2023.

Bloise, A., Fornero, E., Belluso, E., Barrese, E., and Rinaudo, C.: Synthesis and characterization of tremolite asbestos fibres, Eur. J. Mineral., 20, 1027–1033, 2008.

Bloise, A., Catalano, M., Barrese, E., Gualtieri, A.F., Bursi Gandolfi, N., Capella, S., and Belluso, E.: TG/DSC study of the thermal behaviour of hazardous mineral fibres, J. Therm. Anal. Calorim., 123, 2225–2239, 2016.

Bloise, A., Catalano, M., Critelli, T., Apollaro, C., and Miriello, D.: Naturally occurring asbestos: potential for human exposure, San Severino Lucano (Basilicata, Southern Italy), Environ. Earth Sci., 76, 648, https://doi.org/10.1007/s12665-017-6995-9, 2017.

Bloise, A., Catalano, M., and Gualtieri, A. F.: Effect of grinding on chrysotile, amosite and crocidolite and implications for thermal treatment, Minerals, 8, 135, https://doi.org/10.1007/s12665-017-6995-9, 2018a.

Bloise, A., Kusiorowski, R., and Gualtieri, A. F.: The effect of grinding on tremolite asbestos and anthophyllite asbestos, Minerals, 8, https://doi.org/10.3390/min8040135, 2018b.

Cannat, M., Bideau, D., and Bougault, H.: Serpentinized peridotites and gabbros in the Mid-Atlantic Ridge axial valley at 15° 37' N and 16° 52' N, Earth Planet. Sc. Lett., 109, 87–106, 1992.

Décret 96-1133: Décret 96-1133 du 24 dècembre 1996 relatif à l'interdiction de l'amiante, pris en application du code du travail et du code de la consommation, 96–1133, 1996.

Di Giuseppe, D., Perchiazzi, N., Brunelli, D., Giovanardi, T., Nodari, L., Della Ventura, G., Malferrari, D., Marcia, M., and Gualtieri, A. F.: Occurrence and characterization of tremolite asbestos from the Mid Atlantic Ridge. Sci. Rep., 11, 6285, https://doi.org/10.1038/s41598-021-85576-w, 2021.

Dondi, M., Raimondo, M., and Zanelli, C.: Clays and bodies for ceramic tiles: Reappraisal and technological classification, Appl. Clay Sci., 96, 91–109, 2014.

EC 2006/1907: Regulation (EC) N. 1907/2006 of the European Parliament and of the Council of 18 December 2006 Concerning the Registration, Evaluation, Authorisation and Restriction of Chemicals (REACH), Establishing a European Chemicals Agency, Amending Directive 1999/45/EC and Repealing Council Regulation (EEC) N. 793/93 and Commission Regulation (EC) N. 1488/94 As Well As Council Directive 76/769/EEC and Commission Directives 91/155/EEC, 93/67/EEC, 93/105/EC and 2000/21/EC, 2006.

Ernst, W. G. and Liu, J.: Experimental phase-equilibrium study of Al-and Ti-contents of calcic amphibole in MORB–A semiquantitative thermobarometer, Am. Mineral., 83, 952–969, 1998.

Földvári, M.: Handbook of thermogravimetric system of minerals and its use in geological practice, Occasional papers of the Geological Institute of Hungary, Geological Inst. of Hungary, Budapest, ISBN 978-963-671-288-4, 2011.

Gemmi, M., Mugnaioli, E., Gorelik, T. E., Kolb, U., Palatinus, L., Boullay, P., Hovmöller, S., and Abrahams, J. P.: 3D electron diffraction: the nanocrystallography revolution, ACS Central Sci., 5, 1315–1329, 2019.

Gesetz 162/1993: Gesetz zu dem Übereinkommen Nr. 162 der Internationalen Arbeitsorganisation vom 24. Juni 1986 über Sicherheit bei der Verwendung von Asbest, 1993.

Gualtieri, A. F. and Tartaglia, A.: Thermal decomposition of asbestos and recycling in traditional ceramics, J. Eur. Ceram. Soc., 20, 1409–1418, 2000.

Gualtieri, A. F., Gandolfi, N. B., Pollastri, S., Rinaldi, R., Sala, O., Martinelli, G., Paoli, T., Bacci, F., Viani, A., and Vigliaturo, R.: Assessment of the potential hazard represented by natural raw materials containing mineral fibres–The case of the feldspar from Orani, Sardinia (Italy), J. Hazard. Mater., 350, 76–87, 2018a.

Gualtieri, A. F., Pollastri, S., Bursi Gandolfi, N., and Gualtieri, M. L.: In vitro acellular dissolution of mineral fibres: A comparative study, Sci. Rep., 8, 7071, https://doi.org/10.1038/s41598-018-25531-4, 2018b.

Gualtieri, A. F., Lassinantti Gualtieri, M., Scognamiglio, V., and Di Giuseppe, D.: Human health hazards associated with asbestos in building materials, Ecological and health effects of building materials, Springer, 297–325, https://doi.org/10.1007/978-3-030-76073-1_16, 2022.

Gualtieri, A. F., Leoncini, M., Fantone, S., Di Valerio, S., Tossetta, G., Procopio, A. D., Marzioni, D., Pugnaloni, A., Bassi, A. M., Almonti, A., Mirata, S., Vernazza, S., Tirendi, S., Marengo, B., Traverso, N., Passalacqua, M., Scarfì, S., Raneri, S., Fornasini, L., Bersani, D., Ballirano, P., Pacella, A., Bloise, A., Ottaviani, M. F., Mattioli, M., Giordani, M., Della Ventura, G., and Perchiazzi, N.: PRIN 2017 Fibres-A Multidisciplinary Mineralogical, Crystal-Chemical and Biological Project. What have we learned after four years of research?, Per. Min., 92, 143–158, 2023a.

Gualtieri, A. F., Malferrari, D., Di Giuseppe, D., Scognamiglio, V., Sala, O., Gualtieri Lassinanntti, M., Bersani, D., Fornasini, L., and Mugnaioli, E.: There is plenty of asbestos at the bottom. The case of magnesite raw material contaminated with asbestos fibres, Sci. Total Environ., 898, 166275, https://doi.org/10.1016/j.scitotenv.2023.166275, 2023b.

Guggenheim, S. and Koster Van Groos, A. F. K.: Baseline Studies of the Clay Minerals Society Source Clays: Thermal Analysis, Clay. Clay Miner., 49, 433–443, 2001.

Hawthorne, F. C. and Grundy, H. D.: The crystal chemistry of the amphiboles: IV. X-ray and neutron refinements of the crystal structure of tremolite, Can. Mineral. 14, 334–345, 1976.

Hoeck, V., Koller, F., Meisel, T., Onuzi, K., and Kneringer, E.: The Jurassic South Albanian ophiolites: MOR- vs. SSZ-type ophiolites, Lithos, 65, 143–164, 2002.

Huang, E., Chen, C. H., Huang, T., Lin, E. H., and Xu, J. A.: Raman spectroscopic characteristics of Mg-Fe-Ca pyroxenes, Am. Mineral., 85, 473–479, 2000.

Hytönen, K. and Ojanperä, P.: Four tremolites from carbonate rocks of Finland, B. Geol. Soc. Finland, 48, 63–69, 1976.

Iyer, K., Austrheim, H., John, T., and Jamtveit, B.: Serpentinization of the oceanic lithosphere and some geochemical consequences: Constraints from the Leka Ophiolite Complex, Norway, Chem. Geol., 249, 66–90, 2008.

ISO (International Standard Organization): Air quality. Bulk materials. Part 1: Sampling and qualitative determination of asbestos in commercial bulk materials 22262-1, Geneva, Switzerland, 2012.

ISO (International Standard Organization): Air quality. Bulk materials. Part 2: Sampling and qualitative determination of asbestos in commercial bulk materials 22262-2, Geneva, Switzerland, 2014.

ISO (International Standard Organization): Ambient air determination of numerical concentration of inorganic fibrous particles scanning electron microscopy method 14966, Geneva, Switzerland, 2019.

Italian Ministry of Health: Decreto Ministero Sanità Normative e metodologie tecniche di applicazione dell'art. 6, comma 3, dell'art. 12, comma 2, della legge 27 marzo 1992, n. 257, relativa alla cessazione dell'impiego dell'amianto, 6 settembre 1994 (in Italian).

Italian Law n. 257/92 (Legge 27 marzo 1992, n. 257 – Norme relative alla cessazione dell'impiego dell'amianto). In Suppl. Ord. alla Gazzetta Ufficiale 87 del 13 aprile 1992.

Karipi, S., Tsikouras, B., and Hatzipanagiotou, K.: The petrogenesis and tectonic setting of ultramafic rocks from Iti and Kallidromon Mountains, continental cental Greece: Vestiges of the Pindos Ocean, Can. Mineral., 44, 267–287, 2006.

Krzemnicki, M. S.: Diopside needles as inclusions in demantoid garnet from Russia: A Raman microspectrometric study, Gems Gemol., 35, 192–195, 1999.

Külah, T., Kadir, S., Erkoyun, H., Huggett, J., and Atabey, E.: Occurrence of Fibrous Chrysotile and Tremolite in the Çankiri and Ankara Regions, Central Anatolia, Turkey, Clay. Clay Miner., 66, 146–172, 2018.

L'vov, B. V. and Ugolkov, V. L.: Kinetics and mechanism of dehydration of kaolinite, muscovite and talc analyzed thermogravimetrically by the third-law method, J. Therm. Anal. Calorim., 82, 15–22, 2005.

Mackenzie, R. C.: Differential Thermal Analysis, Academic Press, edited by: Mackenzie R. C., London and New York, 1970.

Malferrari, D., Di Giuseppe, D., Scognamiglio, V., and Gualtieri, A.: Commercial brucite, a worldwide used raw material deemed safe, can be contaminated by asbestos, Per. Min., 90, 317–324, 2021.

Malinconico, S., Paglietti, F., Serranti, S., Bonifazi, G., and Lonigro, I.: Asbestos in soil and water: A review of analytical techniques and methods, J. Hazard. Mater., 436, 129083, https://doi.org/10.1016/j.jhazmat.2022.129083, 2022.

Mugnaioli, E., Gorelik, T., and Kolb, U.: "Ab initio" structure solution from electron diffraction data obtained by a combination of automated diffraction tomography and precession technique, Ultramicroscopy, 109, 758–765, 2009.

National Institute for Occupational Safety and Health (NIOSH): Criteria for a Recommended Standard for Occupational Exposure to Asbestos, Federal Register, 1972.

Nicolas, A., Meshi, A., Boudier, F., Jousselin, D., and Muceku, B.: Mylonites in ophiolite of Mirdita (Albania): Oceanic detachment shear zone, Geosphere, 13, 136–154, 2017.

Nozaka, T. and Fryer, P.: Alteration of the Oceanic Lower Crust at a Slow-spreading Axis: Insight from Vein-related Zoned Halos in Olivine Gabbro from Atlantis Massif, Mid-Atlantic Ridge, J. Petrol., 52, 643–664, 2011.

Pacella, A., Andreozzi, G. B., Ballirano, P., and Gianfagna, A.: Crystal chemical and structural characterization of fibrous tremolite from Ala di Stura (Lanzo Valley, Italy), Period. Mineral., 77, 51–62, 2008.

Palatinus, L., Brázda, P., Jelínek, M., Hrdá, J., Steciuk, G., and Klementová, M.: Specifics of the data processing of precession electron diffraction tomography data and their implementation in the program PETS2.0, Acta Crystallogr. B, 75, 512–522, 2019.

Rinaudo, C. and Croce, A.: Micro-raman spectroscopy, a powerful technique allowing sure identification and complete characterization of asbestiform minerals, Appl. Sci., 9, 3092, https://doi.org/10.3390/app9153092, 2019.

Rutstein, M. S. and Yund, R. A.: Unit-cell parameters of synthetic diopside-hedenbergite solid solutions, Am. Mineral., 54, 238–245, 1969.

Saccani, E. and Tassinari, R.: The role of MORB and SSZ magmatypes in the formation of Jurassic ultramafic cumulates in the Mirdita ophiolites (Albania) as deduced from chromian spinel and olivine chemistry, Ofioliti, 40, 37–56, 2015.

Salamatipour, A., Mohanty, S. K., Pietrofesa, R. A., Vann, D. R., Christofidou-Solomidou, M., and Willenbring, J. K.: Asbestos fiber preparation methods affect fiber toxicity, Environ. Sci. Technol. Lett., 3, 270–274, 2016.

Schneider, T., Jørgensen, O., Davies, L. S., Buchanan, D., Burdett, G., Tempelman, J., Puledda, S., and Paoletti, L.: Development of a method for the determination of low contents of asbestos fibres in bulk material, Analyst, 123, 1393–1400, 1998.

Siegrist Jr., H. G. and Wylie, A. G.: Characterizing and discriminating the shape of asbestos particles, Environ. Res., 23, 348–361, 1980.

Spurny, K. R., Stöber, W., Opiela, H., and Weiss, G.: On the problem of milling and ultrasonic treatment of asbestos and glass fibers in biological and analytical applications, Am. Ind. Hyg. Assoc. J., 41, 198–203, 1980.

Stripp, G. R., Field, M., Schumacher, J. C., Sparks, R. S. J., and Cressey, G.: Post-emplacement serpentinization and related hydrothermal metamorphism in a kimberlite from Venetia, South Africa, J. Metamorph. Geol., 24, 515–534, 2006.

Taufiq-Yap, Y. H., Nur-Faizal, A. R., Sivasangar, S., Hussein, M. Z., and Aishah, A.: Modification of Malaysian dolomite using mechanochemical treatment via different media for oil palm fronds gasification: Potential of Malaysian dolomite as a gasification catalysts, Int. J. Energ. Res., 38, 1008–1015, 2014.

Thompson, R. M. and Downs, R. T.: The crystal structure of diopside at pressure to 10 GPa, Am. Mineral., 93, 177–186, 2008.

Tribaudino, M., Mantovani, L., Bersani, D., and Lottici, P. P.: Raman spectroscopy of (Ca, Mg) $MgSi_2O_6$ clinopyroxenes, Am. Mineral., 97, 1339–1347, 2012.

Verkouteren, J. R. and Wylie, A. G.: The tremolite-actinolite-ferro–actinolite series: Systematic relationships among cell parameters, composition, optical properties, and habit, and evidence of discontinuities, Am. Mineral., 85, 1239–1254, 2000.

Wang, A., Jolliff, B. L., Haskin, L. A., Kuebler, K. E., and Viskupic, K. M.: Characterization and comparison of structural and compositional features of planetary quadrilateral pyroxenes by Raman spectroscopy, Am. Mineral., 86, 790–806, 2001.

Wesołowski, M.: Thermal decomposition of talc: A review, Thermochim. Acta, 78, 395–421, 1984.

World Health Organization (WHO): Asbestos and Other Natural Mineral Fibres. Environmental Health Criteria, 53. World Health Organization: Geneva, Switzerland, p. 194, 1986.

Wylie, A. G. and Schweitzer, P.: The effects of sample preparation and measuring techniques on the shape and shape characterization of mineral particles: the case of wollastonite, Environ. Res., 27, 52–73, 1982.

Zhao, M. S., Chen, Y. X., and Zheng, Y. F.: Geochemical evidence for forearc metasomatism of peridotite in the Xigaze ophiolite during subduction initiation in Neo-Tethyan Ocean, south to Tibet, Lithos, 380–381, 2021.